PNAS
www.pnas.org

Supplementary Information for:

ZNRF3 functions in mammalian sex determination by inhibiting canonical WNT signalling

Abigail Harris, Pam Siggers, Silvia Corrochano, Nick Warr, Danielle Sagar, Daniel T. Grimes, Makoto Suzuki, Rebecca D. Burdine, Feng Cong, Bon-Kyoung Koo, Hans Clevers, Isabelle Stévant, Serge Nef, Sara Wells, Raja Brauner, Bochra Ben Rhouma, Neïla Belguith, Caroline Eozenou, Joelle Bignon-Topalovic, Anu Bashamboo, Ken McElreavey & Andy Greenfield

Corresponding author: Andy Greenfield
Email: a.greenfield@har.mrc.ac.uk

www.pnas.org/cgi/doi/10.1073/pnas.1801223115

This PDF file includes:

Supplementary Methods

Figs. S1 to S7

Supplementary Methods

Studies of Human Disorders of Sex Development (DSD)

Subjects and Samples. All patients with 46,XY DSD met the revised criteria of the Pediatric Endocrine Society (LWPES)/European Society for Paediatric Endocrinology (ESPE). This study was approved by the local French ethical committee (2014/18NICB – registration number IRB00003835) and consent to genetic testing was obtained from adult probands or from the parents when the patient was under 18 years. Patient ancestry was determined by self-reporting, based on responses to a personal questionnaire, which asked questions pertaining to the birthplace, languages and self-reported ethnicity of the participants, their parents and grandparents. Genes known to be involved in 46,XY DSD were screened for mutations in the XY DSD cohort and high resolution aCGH was performed on all cases and indicated normal ploidy in all cases.

Whole-exome sequencing. Exon enrichment was performed with Agilent SureSelect Human All Exon V4. Paired-end sequencing was performed on the Illumina HiSeq2000 platform with TruSeq v3 chemistry. Read files (fastq) were generated from the sequencing platform via the manufacturer's proprietary software. Reads were mapped with the Burrows-Wheeler Aligner (1), and local realignment of the mapped reads around potential insertion/deletion (indel) sites was carried out with GATK version 1.6 (2). Duplicate reads were marked with Picard version 1.62 (http://broadinstitute.github.io/picard/). Additional BAM file

manipulations were performed with Samtools (0.1.18; (3)). SNP and indel variants were called with the GATK Unified Genotyper for each sample. SNP novelty was determined against dbSNP138. Novel variants were analyzed by a range of web-based bioinformatics tools with the EnsEMBL SNP Effect Predictor (http://www.ensembl.org/Homo_sapiens/Tools/VEP/). All variants were screened manually against the Human Gene Mutation Database Professional Biobase (http://www.biobase-international.com/product/hgmd/). *In silico* analysis was performed to determine the potential pathogenicity of the variants. Potentially pathogenic variants were verified with classic Sanger sequencing.

Investigation of ZNRF3 activity in Zebrafish

To determine the effect of these variants on ZNRF3 function, we used an overexpression assay in zebrafish that assesses the impact of low (12.5 pg) and high (50 pg) doses of injected *ZNRF3* messenger RNA (mRNA) on early embryogenesis. Injection of ZNRF3-WT at low levels caused no phenotypes but at higher doses ZNRF3-WT induced dorsalization in a proportion of embryos (Fig. 4vi, n=20/40) and cyclopia was observed occasionally (n=7/40). These phenotypes are indicative of reduced Wnt/beta-catenin signals and abnormal Wnt/PCP, respectively (4-6). By contrast, overexpression of the ZNRF3-S554N variant induced no significant defects at either low (Fig. 4iii, n=47/49) or high (n=30/33) doses (Fig. 4vii). The inability to induce phenotypes when overexpressed suggests that the ZNRF3-S554N variant is loss-of-function, possibly hypomorphic or null. We then tested ZNRF3-R768G and found

pronounced reduction of anterior structures including the forebrain and eyes at both low (Fig. 4iv, n=54/55) and high (Fig. 4viii, n=33/36) doses. These phenotypes are associated with overactive Wnt/beta-catenin signals (7), supporting a model in which either ZNRF3-R768G acts in a dominant fashion to disrupt endogenous ZNRF3 function or results in ligand-independent activation of Wnt/beta-catenin. Overall, these data suggest that both S554N and R768G ZNRF3 variants impact protein function and predict that both mutations would result in over-activation of Wnt/beta-catenin pathways in endogenous, whole organismal contexts.

Zebrafish assays: Plasmids containing ZNRF3-HA were mutagenized using the QuikChange II Site-Directed Mutagenesis kit (Agilent) to incorporate S554N and R768G point mutations. Plasmids were linearized with PmeI (NEB) and mRNA was synthesized using T7 enzyme and the mMESSAGE mMACHINE T7 transcription kit (Thermo Fisher Scientific). mRNA was injected into the blastomeres of 1-cell stage zebrafish embryos and phenotypic consequences were determined after embryos were raised at 28^{o}C. Images were taken with a Leica M205FA microscope with a DFC365 FX camera attachment (Leica Microsystems). Zebrafish animal care protocols were adhered to in accordance with the guidelines of Princeton's Institutional Animal Care and Use Committee (IACUC). Wild-type zebrafish of the WIK strain were used.

TOPFLASH Assays in KGN Cells

To assay the ability of ZNRF3 proteins to modulate the canonical WNT pathway, we used the TOPFlash-TCF reporter plasmid. Transient gene expression assays were performed in 96 well plates (Nunc) using KGN (ovarian granulosa cell tumor) cells, FuGENE 6 (Roche) transfection reagent and a Dual-Luciferase reporter assay system (Promega) with pRL-CMV Renilla luciferase (Promega) expression as a marker of transfection efficiency. *ZNRF3* expression vectors (10 ng/well) were co-transfected with reporter and vector containing Renilla luciferase (10 ng/well). Cells were lysed 48 hours later and luciferase assays were performed (Dual Luciferase Reporter Assay system, Promega) using a Centrox3 LB960 (Berthold Technologies). All data were standardized for Renilla luciferase activity. Results are shown as the mean ± SEM of at least four independent experiments, each performed at least in quadruplicate.

The results of the luciferase assays were compared for their statistical significance by calculating two-tailed Student's *t*-Test using GraphPad Prism software. 95% confidence interval was calculated using the mean difference between the two groups being tested. The data for each of the groups tested and their *t* values, along with degrees of freedom (df), standard error of difference were taken into account to calculate the *P*-values and determine the statistical significance.

Single-cell RNAseq

Somatic cells from the developing gonads were purified by FACS from CD1 XX and XY Tg(*Nr5a1*-GFP) animals (8, 9) at five different developmental stages (10.5 - 13.5 dpc and 16.5 dpc). Sorted GFP-positive cells were isolated, RNA-processed with the Fluidigm C1 Autoprep system (small-size IFC) and sequenced at an average depth of 15M reads per cell with the Illumina Hiseq2000 (100bp, paired-end reads). Reads were mapped on the mouse reference genome (from GENCODE, genome version GRCm38.p3, annotation version M4) using GemTools and SamTools. Expression values were normalised with RPKMs (Reads Per Kilobase of exon per Million reads mapped). Classification of the high-quality, single-cell transcriptomes was performed by selection of highly variable genes (method from (10) and hierarchical clustering on principal component analysis. Identification of cell-types was based on enrichment of marker genes in the obtained cell clusters. Graphics were generated with Ggplot2 and figures were prepared with Inkscape.

Primer pairs used in this study for qRT-PCR (5' to 3'):

Znrf3	CAAGGCCAAGAGAGCAGTTC	GCACCCTTCACATACACCAC
Hprt1	CATTATGCCGAGGATTTGGAA	CACACAGAGGGCCACAATGT
Sry	TTATGGTGTGGTCCCGTGGT	GGCCTTTTTTCGGCTTCTGT
Sox9	AAGAAAGACCACCCCGATTACA	CAGCGCCTTGAAGATAGCATT
Axin2	AGTGCAAACTCTCACCCACC	TCGCTGGATAACTCGCTGTC
Lef1	GCGACTTAGCCGACATCAAG	AGGGTCCCTTGTTGTACAGG
Wnt4	GTCTTCGCCGTGTTCTCG	CTCAAGGTTCCGTTTGCACA
Rspo1	GCTCCAACTCTCGGAGACAC	GTCACTGTGCCCAGGTAGGT
Sf1	TTCGTCTGTCTCAAGTTCCTCATC	CCTTTACGAGGCTGTGGTTGTT
Oct4	CTCAGCCTTAAGAACATGTG	TTCTCTTGTCTACCTCCCTT

Supplementary Figures

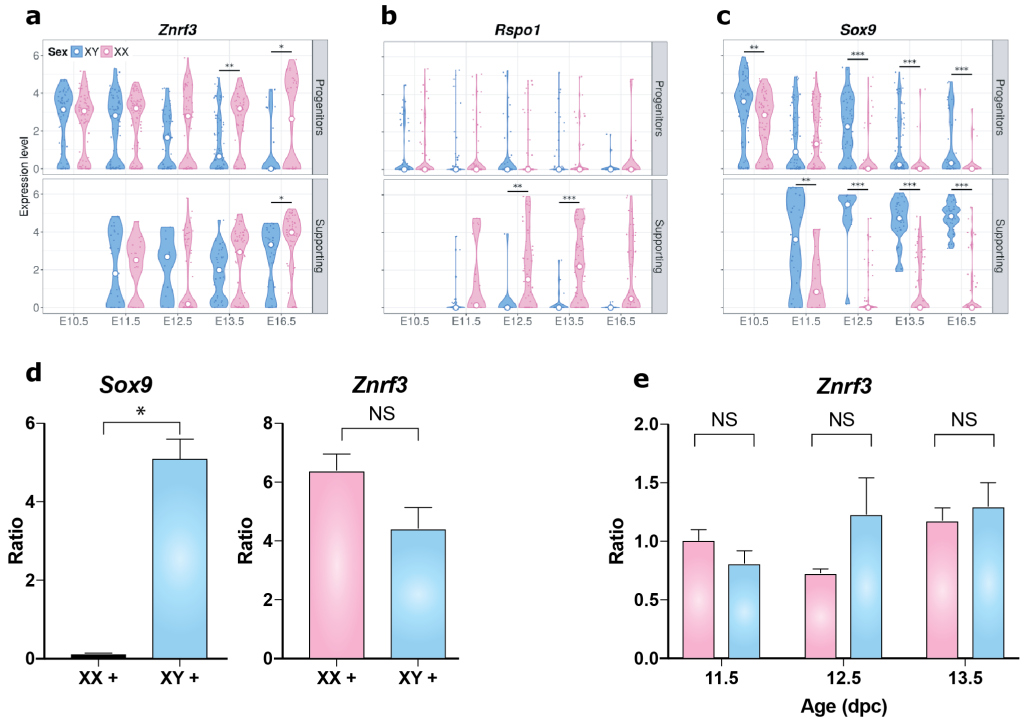

Fig. S1

Figure S1. *Znrf3* expression in the developing mouse gonad. A-C) Violin plots showing the expression of genes of interest in the progenitor and supporting cell lineages in both sexes between 10.5 dpc to 16.5 dpc (E10.5 to E16.5) determined by single-cell RNAseq analysis of *Sf1*-positive somatic cells. The width of the violin indicates the proportion of cells. Expression values are log-transformed reads per kilobase of transcript per million mapped reads (RPKM); small points represent individual cells and the white point is the median of expression. Statistical analyses were performed using the Mann Whitney test. For more details of methodology and analyses see Stévant et al (11). D)

Quantitation of *Znrf3* expression in *Sf1*-positive cells isolated from XY (blue) and XX (red) gonads at 11.5 dpc using FACS sorting; *Sox9* data are included as a control. E) Quantitation of *Znrf3* expression in whole XY (blue) and XX (red) gonads at 11.5, 12.5 and 13.5 dpc. *$P \leq 0.05$; **$P \leq 0.01$; ***$P \leq 0.0001$ (Mann Whitney test).

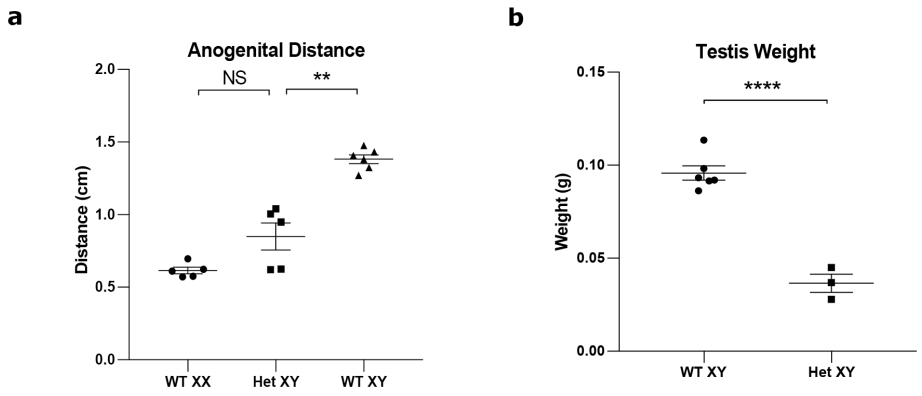

Fig. S2

Figure S2. Gonadal and genital defects in adult *Znrf3*$^{-/+}$ heterozygous mutants on the B6.Y^{AKR} genetic background. A) Anogenital distance is significantly reduced in XY heterozygous (het) mutants compared to XY wild-type (WT) controls. B) Testis weights in heterozygous mutants are significantly lower than controls. ***P*≤ 0.01; *****P*≤ 0.00001 (Student's *t*-test).

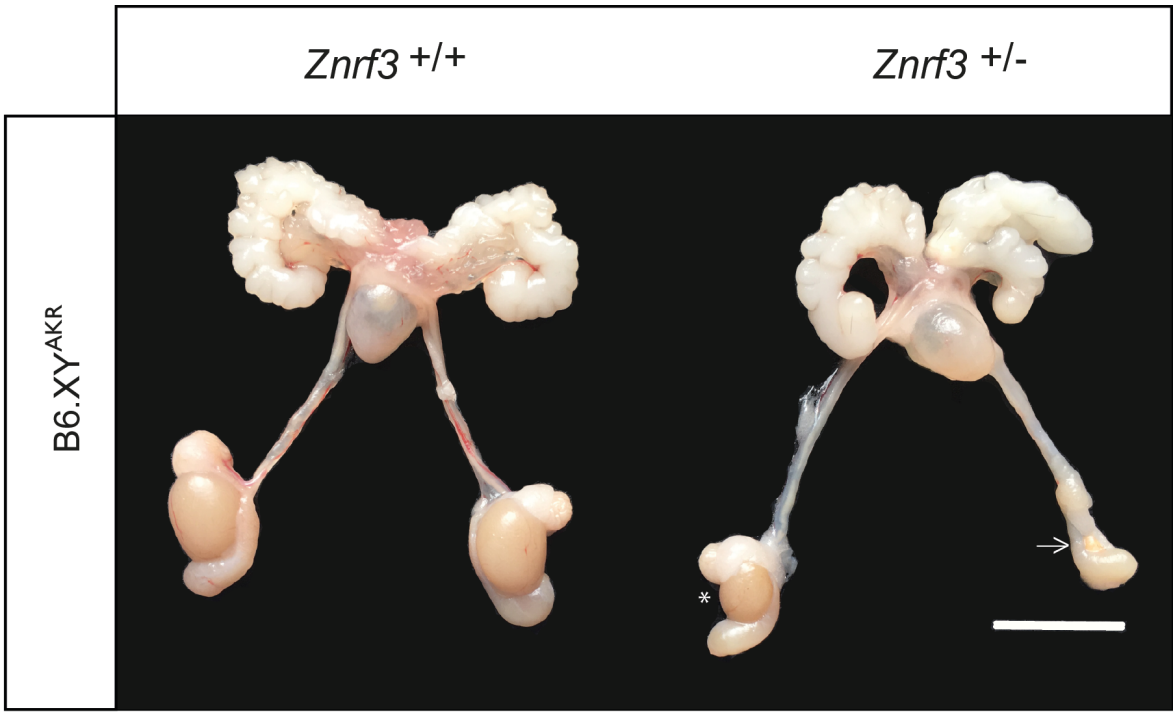

Fig. S3

Figure S3. Internal genital abnormalities of an adult *Znrf3*$^{-/+}$ heterozygous mutant. The control male (B6.Y^{AKR} +/+, left) has two prominent testes and normal reproductive tract structure. The heterozygous mutant male (B6.Y^{AKR} +/-) has a hypoplastic testes on the left as viewed (asterisk) and a very small ovary-like gonad on the right as viewed (arrow). Reproductive tracts appear otherwise masculinised. Scale bar, 1 cm.

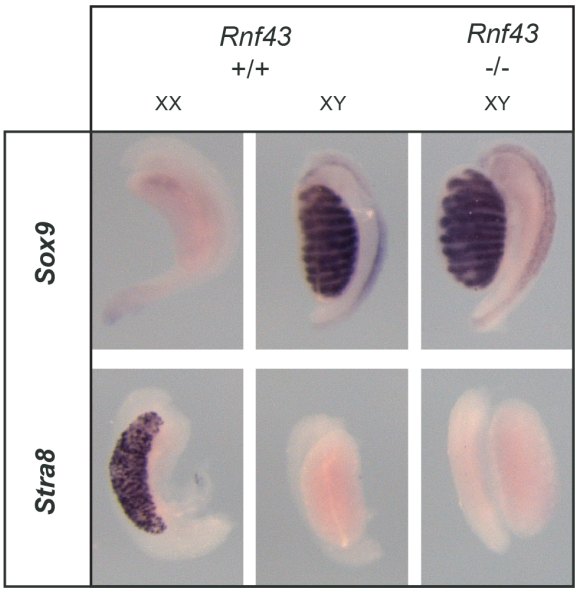

Fig. S4

Figure S4. Fetal (14.5 dpc) XY gonads lacking the WNT-antagonist RNF43 develop normally. Mutant XY *Rnf43* $^{-/-}$ gonads (far right) exhibit normal testis cord formation, *Sox9* expression and absence of *Stra8,* like control XY wild-type (+/+) gonads.

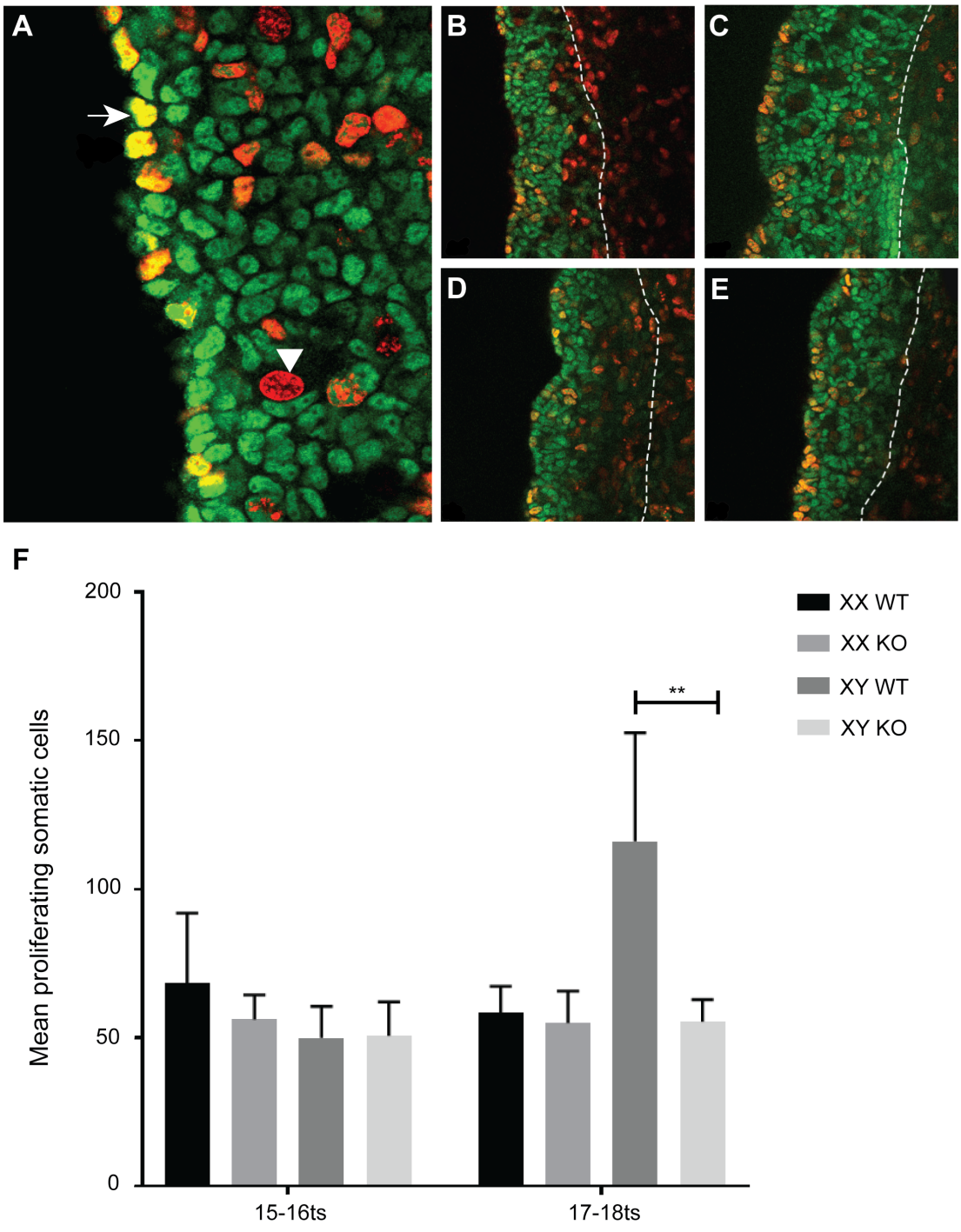

Figure S5. Somatic cell proliferation in wild-type and *Znrf3*$^{-/-}$ gonads at 11.0 and 11.5 dpc. (A) Higher magnification image (x40) depicting the distinct types of

proliferating cell. GATA4 (green) is used to label the somatic cells of the gonad; EdU (red) marks cells that have undergone S-phase (or derivatives of these) i.e. dividing cells. The large red nucleus (arrowhead) is EdU-positive but GATA4-negative i.e. a germ cell. Only cells labelled red and green (yellow/orange) (arrow) are counted; (B) Representative XX wild-type (17-18 ts) gonad (x20); (C) XY wild-type (17-18 ts) gonad (x20); (D) XX *Znrf3*$^{-/-}$ (17-18 ts) gonad (x20); (E) XY *Znrf3*$^{-/-}$ (17-18 ts) gonad (x20); (F) Comparison of mean numbers of proliferating somatic cells in wild-type or *Znrf3*$^{-/-}$ gonads at 15-16 ts or 17-18 ts. ** = $p \leq 0.01$ (n= 5-6).

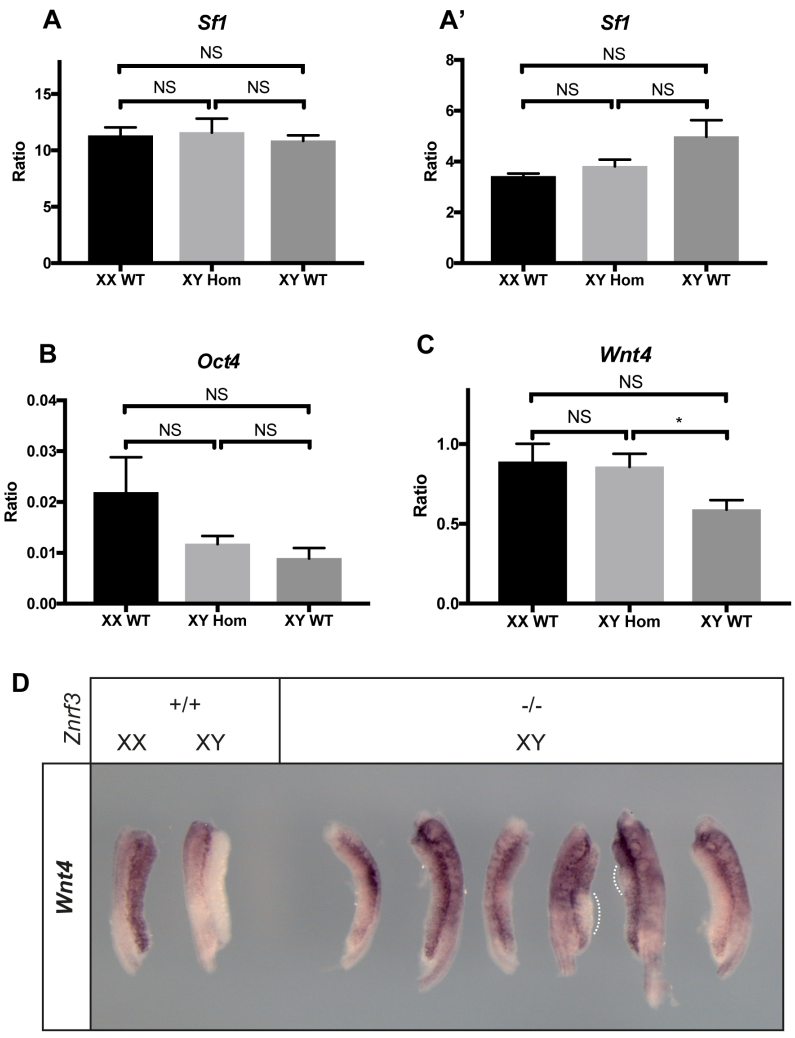
A
Sf1
NS
NS
NS
Ratio
15
10
5
0
XX WT
XY Hom
XY WT
A'
Sf1
NS
NS
NS
Ratio
8
6
4
2
0
XX WT
XY Hom
XY WT
B
Oct4
NS
NS
NS
Ratio
0.04
0.03
0.02
0.01
0.00
XX WT
XY Hom
XY WT
C
Wnt4
NS
NS
*
Ratio
1.0
0.5
0.0
XX WT
XY Hom
XY WT
D
Znrf3
+/+
XX
XY
-/-
XY
Wnt4

Fig. S6

Figure S6. Expression analyses of XY gonads lacking ZNRF3. A, A') *Sf1* (*Nr5a1*) expression is unaffected in gonads lacking *Znrf3* at 11.5 dpc (A) and 12.5 dpc (A'). B) *Oct4* expression is unaffected at 12.5 dpc. C) qRT-PCR reveals that gonadal *Wnt4* expression in XY *Znrf3* homozygous mutants is elevated at 11.5 dpc (18 ts) in comparison to wild-type (WT) XY controls. D) WMISH analysis of *Wnt4* expression in gonads at around 12.5 dpc reveals ectopic expression in XY *Znrf3* homozygotes. XX controls show strong gonadal *Wnt4* signal, whilst XY controls lack *Wnt4*. Six mutant XY gonads exhibit variable *Wnt4* expression, with some region-specific activation. Dotted lines indicate regions not exhibiting high levels of *Wnt4*. Several XY mutant gonads exhibit higher levels of *Wnt4* in the gonadal 'medullary' region, adjacent to the mesonephros.

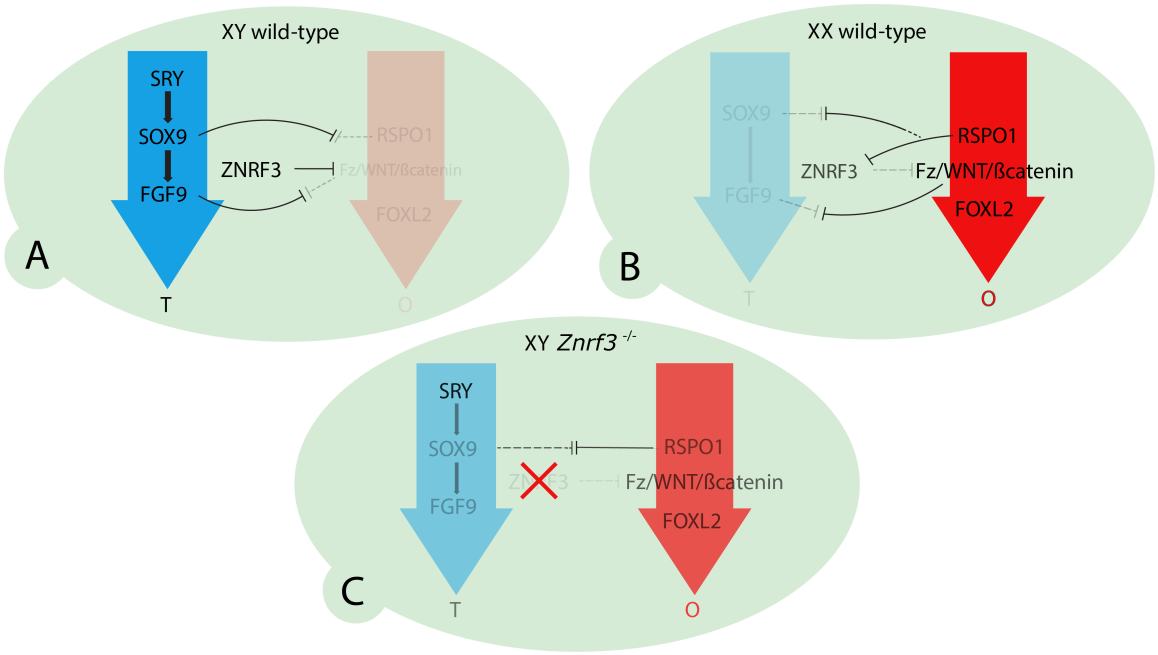

Fig. S7

Figure S7. Model of ZNRF3 function during sex determination. A) Testis-determining (T) ZNRF3 activity in the supporting cell lineage of the wild-type XY gonad inhibits WNT/β-catenin signalling by removal of Frizzled receptor (Fz). This supports the establishment of the FGF9-SOX9 axis in driving Sertoli cell differentiation. B) In XX gonads, a double-negative regulatory module operates: higher levels of *RSPO1* transcription result in inhibition of ZNRF3 activity, resulting in ZNRF3's ability to inhibit Fz/WNT/β-catenin signalling being greatly reduced. This results in the dominance of the ovary-determining (O) RSPO1/WNT4/FOXL2 network. C) In the XY *Znrf3* knockout, loss of ZNRF3 allows RSPO1/WNT4/Fz/β-catenin to suppress *SOX9* transcription and inhibit Sertoli cell differentiation, despite the continued presence of SRY. SRY-dependent promotion of *SOX9* transcription may sometimes tilt the balance

towards to the testicular fate in XY mutants, generating an inherently unstable sex-determining network, accounting for the phenotypic variability observed.

REFERENCES

1. Li H & Durbin R (2010) Fast and accurate long-read alignment with Burrows-Wheeler transform. *Bioinformatics* 26(5):589-595.
2. Zhu P, *et al.* (2014) OTG-snpcaller: an optimized pipeline based on TMAP and GATK for SNP calling from ion torrent data. *PLoS One* 9(5):e97507.
3. Li H, *et al.* (2009) The Sequence Alignment/Map format and SAMtools. *Bioinformatics* 25(16):2078-2079.
4. Topczewski J, *et al.* (2001) The zebrafish glypican knypek controls cell polarity during gastrulation movements of convergent extension. *Dev Cell* 1(2):251-264.
5. Heisenberg CP & Nusslein-Volhard C (1997) The function of silberblick in the positioning of the eye anlage in the zebrafish embryo. *Dev Biol* 184(1):85-94.
6. Hikasa H & Sokol SY (2013) Wnt signaling in vertebrate axis specification. *Cold Spring Harb Perspect Biol* 5(1):a007955.
7. van de Water S, *et al.* (2001) Ectopic Wnt signal determines the eyeless phenotype of zebrafish masterblind mutant. *Development* 128(20):3877-3888.
8. Nef S, *et al.* (2005) Gene expression during sex determination reveals a robust female genetic program at the onset of ovarian development. *Dev Biol* 287(2):361-377.
9. Stallings NR, *et al.* (2002) Development of a transgenic green fluorescent protein lineage marker for steroidogenic factor 1. *Mol Endocrinol* 16(10):2360-2370.
10. Brennecke P, *et al.* (2013) Accounting for technical noise in single-cell RNA-seq experiments. *Nat Methods* 10(11):1093-1095.
11. Stevant I, *et al.* (2018) Deciphering Cell Lineage Specification during Male Sex Determination with Single-Cell RNA Sequencing. *Cell reports* 22(6):1589-1599.